Research Article

A Large-Scale Synthesis and Characterization of Quaternary $CuIn_xGa_{1-x}S_2$ Chalcopyrite Nanoparticles via Microwave Batch Reactions

Chivin Sun,[1] Richard D. Westover,[1] Gary Long,[1] Cyril Bajracharya,[1] Jerry D. Harris,[2] Alex Punnoose,[3] Rene G. Rodriguez,[1] and Joshua J. Pak[1]

[1] *Department of Chemistry, Idaho State University, Pocatello, ID 83209, USA*
[2] *Department of Chemistry, Northwest Nazarene University, Nampa, ID 83686, USA*
[3] *Department of Physics, Boise State University, Boise, ID 83725, USA*

Correspondence should be addressed to Joshua J. Pak, pakjosh@isu.edu

Various quaternary $CuIn_xGa_{1-x}S_2$ ($0 \leq x \leq 1$) chalcopyrite nanoparticles have been prepared from molecular single-source precursors via microwave decomposition. We were able to control the nanoparticle size, phase, stoichiometry, and solubility. Depending on the choice of surface modifiers used, we were able to tune the solubility of the resulting nanoparticles. This method has been used to generate up to 5 g of nanoparticles and up to 150 g from multiple batch reactions with excellent reproducibility. Data from UV-Vis, photoluminescence, X-ray diffraction, TEM, DSC/TGA-MS, and ICP-OES analyses have shown high reproducibility in nanoparticle size, composition, and bandgap.

1. Introduction

For nearly three decades, chalcopyrite $CuIn_{0.7}Ga_{0.3}Se_2$ (CIGS) and related materials have attracted much interest due to their potential applications in photovoltaic and other optoelectric devices [1–5]. Many thin film PV devices of CIGS set respectable power conversion efficiency of about 20% [6, 7]. In recent years, there have been increasing reports on using colloidal I–III–VI nanoparticle suspensions, composites, and inks to prepare PV devices. Solution processing strategies such as spin coating [8–10] and ink printing [1, 2, 4] are being explored for large areas of CIGS while lowering the overall costs.

One of the key stoichiometric requirements is to consistently maintain In/Ga ratio to 0.7/0.3 from batch to batch. Previously, we reported the efficient syntheses of quaternary $CuIn_xGa_{1-x}S_2$ ($0 \leq x \leq 1$) chalcopyrite nanoparticles with precise stoichiometric control by decomposition of a mixture of two I–III bimetallic single-source precursors

(SSPs), $(Ph_3P)_2Cu(\mu\text{-}SEt)_2In(SEt)_2$ (**1**), and $(Ph_3P)_2Cu(\mu\text{-}SEt)_2Ga(SEt)_2$ (**2**), in the presence of 1,2-ethanedithiol via microwave irradiation [11].

Use of SSPs in preparation of nanomaterials presents distinct advantages such as precise control of reaction conditions and stoichiometry as SSPs contain all necessary elements in a single molecule. Despite the obvious advantages of SSPs, to our knowledge, no studies have been conducted using combinations of SSPs to form soluble and insoluble ternary and quaternary chalcopyrite nanoparticles.

Microwave-assisted preparation of nanoparticles from SSPs offers advantages over traditional thermolysis as microwave provides rapid heating as well as greater homogeneity in the overall reaction temperature [12]. This usually allows for the preparation of nanoparticles with increased size control [13], dramatic decreases in reaction times, improved product purities, and reactions exhibiting good reproducibility and high yields [14, 15].

In our studies, the nanoparticles were produced using 1,2-ethanedithiol as surface stabilizer and cross-linker of SSPs. 1,2-Ethanedithiol undergoes thiolate ligand exchange reactions, which produce random copolymers of SSPs. This formation of random copolymers between SSPs **1** and **3** is a important requirement for us to control In-Ga ratio in nanoparticles. 1,2-Ethanedithiol also cross-links nanoparticles, and the resulting organic-nanoparticle composite precipitates out of reaction solution as insoluble micron-sized clusters [14]. Although the resulting material exhibited excellent size, stoichiometry, and bandgap control, these micron-sized clusters are not suitable for some solution-based thin film processing methods, which require highly soluble nanoparticles in common organic solvents. Therefore, the ability to modulate organic constituents on these CIGS nanoparticles whether to improve solubility or to add functionality through a hybrid composite is important. Judicious use of organic cross-linking agents in conjunction with other monothiols can control the solubility of resulting nanoparticles. The ability to modulate both physical and chemical properties could lead to future applications of these particles in organic-inorganic composites in photovoltaics [16–19], biological investigations [20, 21], and catalysis [22].

The full realization of the potential of these nanoparticles will require synthetic strategies capable of consistently producing nanoparticles on a multigram scale. Despite the obvious needs, scales of tens of milligrams are typical for the production of CIS and CIGS nanoparticles [23–26]. Thus far, the production of these nanoparticles on a gram scale or larger has received limited attention [11, 14, 27–29]. In addition, the preparation of soluble $CuIn_xGa_{1-x}S_2$ nanoparticles with precise stoichiometric control has not been reported to best of our knowledge on any scale.

We recently discovered that the reaction of two SSPs with limited amount of 1,2-ethanedithiol as a cross-linker and excess of 1-hexanethiol as a surface modifier provides a way to tune the solubility from insoluble to soluble nanoparticles while maintaining precise stoichiometric control.

Herein, we report the preparation of quaternary $CuIn_xGa_{1-x}S_2$ $(0 \leq x \leq 1)$ chalcopyrite nanoparticles with tunable bandgap and solubility on scales of up to 150 g with precise stoichiometric control by selectively decomposing mixtures of SSPs **1** and **2** or mixtures of SSPs **3** and **4** (Figure 1) via microwave irradiation.

2. Experimental

2.1. General Considerations. Triphenylphosphine (Ph_3P, 99+%), 1,2-ethanediti ol ($HSCH_2CH_2SH$, 99.8%), benzyl acetate ($C_6H_5CH_2CO_2CH_3$, 99%), gallium (III) chloride ($GaCl_3$, ultradry, 99.999%, metals basis), and indium (III) chloride ($InCl_3$, anhydrous 99.99%, metals basis) were purchased from Alfa Aesar. Ethanethiol (CH_3CH_2SH, 99+ %), 1-hexanethiol ($CH_3(CH_2)_5SH$, 96%), thiophenol (PhSH, 99+%), and copper (I) chloride (CuCl, 99.999%, extra pure, purified) were purchased from Acros Organics. All other solvents (benzene, tetrahydrofuran, diethyl ether, and pentane) were dried and degassed using an Innovative Technology

Inc. solvent purification system (activated alumina, copper catalyst, and molecular sieves columns) before use. All other reagents were obtained from commercial sources and used without further purification. Milestone microwave (Labstation ETHOS EX) was used with a 15 min ramp and a 45 or 60 min hold at desired reaction temperatures. The resulting nanoparticles were characterized using a JEOL 2010 high-resolution transmission electron microscope (HRTEM) with a spatial resolution of 0.194 nm. Powder X-ray diffraction (XRD) patterns were acquired with a Bruker D8 Discover diffractometer using CuKa radiation source and a scintillation detector. Scans were collected for 4 hrs employing a 0.06° step width at a rate of 10 s/step resulting in a 2θ scanning range from 10 to 60°. Absorption spectra of nanoparticles were obtained from UV-Vis data recorded on a Shimadzu UV-Vis scanning (UV-3101PC) spectrophotometer using an integrating sphere module at room temperature. Inductively, coupled plasma-optical emission spectroscopy (ICP-OES) analysis was accomplished by weighing 20 mg of each nanoparticle sample then digesting in concentrated HNO_3 to make a 10 ppm solution. All samples were run within 24 hours of preparing the solution to ensure that the results were consistent. All ICP data were recorded on a Varian 715-ES (ICP-OES with V-groove Nebulizer). Photoluminescence spectra were recorded using a Horiba Jobin Yvon Fluoromax-3 spectrofluorometer with 1 cm path length cells. The cells were cleaned, and samples were prepared with spectroscopic-grade benzene. The thermal degradation of the nanoparticles was characterized using a Mettler Toledo TGA/DSC1 thermal analyzer, connected to a Pfeiffer Vacuum ThermoStar mass spectrometer. Thermal characterization was preformed in an argon environment, with ramp rates of 10–50°C/min from 50°C to 600°C in alumina crucibles.

2.2. Synthesis of Single-Source Precursors (SSPs) [30–33]. $(Ph_3P)_2Cu(\mu\text{-}SEt)_2In(SEt)_2$ (**1**), $(Ph_3P)_2Cu(\mu\text{-}SEt)_2Ga(SEt)_2$ (**2**), $(Ph_3P)_2Cu(\mu\text{-}SPh)_2In(SPh)_2$ (**3**), and $(Ph_3P)_2Cu(\mu\text{-}SPh)_2Ga(SPh)_2$ (**4**) were synthesized according to the literature [30–33].

2.3. General Procedure for the Preparation of $CuIn_xGa_{1-x}S_2$ $(0 \leq x \leq 1)$ Chalcopyrite Nanoparticles [11]. For the general reaction, in a dry Milestone microwave vessel, $(Ph_3P)_2Cu(\mu\text{-}SEt)_2In(SEt)_2$ (SSP **1**, 1.500 g, 1.583 mmoL) and $(Ph_3P)_2Cu(\mu\text{-}SEt)_2Ga(SEt)_2$ (SSP **2**, 1.429 g, 1.583 mmoL) were dissolved in 18 mL of dry benzyl acetate followed by addition of 1,2-ethanedithiol (1.8 mL, 21.46 mmoL). The reaction mixture was stirred at room temperature for 5 min and heated at set temperatures for 1 hour via microwave irradiation. Upon completion, the reaction was cooled to room temperature, and $CuIn_{0.5}Ga_{0.5}S_2$ nanoparticles were recovered by serial precipitation, centrifugation, and washing in CH_3OH to provide yellow to black powder.

*2.4. Preparation of Highly Cross-Linked Quaternary $CuIn_{0.7}Ga_{0.3}S_2$ Chalcopyrite Nanoparticles from SSPs **3** and **4**.* For the general reaction, in a dry Milestone microwave vessel, $(Ph_3P)_2Cu(\mu\text{-}SPh)_2In(SPh)_2$ (**3**, 13.61 g, 11.95 mmoL),
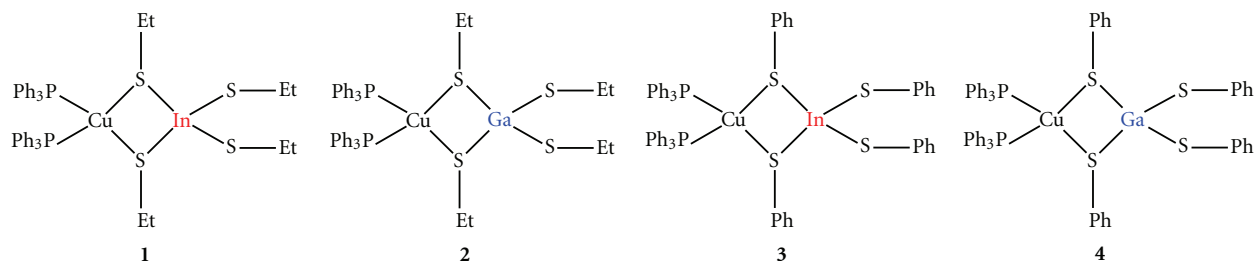
Figure 1: Single-source precursors **1** through **4**.

$(Ph_3P)_2Cu(\mu\text{-}SPh)_2Ga(SPh)_2$ (**4**, 6.43 g, 5.87 mmoL), and 1,2-ethanedithiol (9.72 mL, 115.9 mmoL) were dissolved in 88.0 mL of benzyl acetate. The reaction was heated at reaction temperatures 160, 180, or 200°C for 1 hr. Upon completion, the reaction was cooled to room temperature, and $CuIn_{0.7}Ga_{0.3}S_2$ nanoparticles were recovered by serial precipitation, centrifugation, and washing with CH_3OH to provide black powder. This method has been successfully adapted to prepare up to 5 g of nanoparticles in a single vessel (Figure 2).

2.5. Preparation of Organic Soluble Quaternary $CuIn_xGa_{1-x}S_2$ $(0 \leq x \leq 1)$ Chalcopyrite Nanoparticles. $(Ph_3P)_2Cu(\mu SEt)_2In(SEt)_2$ (**1**, 6.00 grams, 6.33 millimoles) and $(Ph_3P)_2Cu(\mu\text{-}SEt)_2Ga(SEt)_2$ (**2**, 5.71 grams, 6.33 millimoles) were dissolved in 60 mL of benzene, and 1,2-ethanedithiol (1.06 mL, 12.66 millimoles) was added to afford random polymer of **1** and **2**. After stirring at room temperature for 1 hr, the solvent and ethanethiol were removed to afford white solid. The resulting solid was redissolved in benzyl acetate (20 mL) followed by addition of 1-hexanethiol (2.00 mL). The reaction was heated at reaction temperatures between 160 and 200°C for 1 hr. Upon completion, the reaction was cooled to room temperature, and $CuIn_xGa_{1-x}S_2$ $(0 \leq x \leq 1)$ nanoparticles were recovered by serial precipitation, centrifugation, and washing in CH_3OH to provide red to red-black powder.

2.6. Preparation of Organic Soluble Quaternary $CuIn_{0.7}Ga_{0.3}S_2$ Chalcopyrite Nanoparticles. Following general reaction, a combination of two SSPs, $(Ph_3P)_2Cu(\mu\text{-}SEt)_2In(SEt)_2$ (SSP **1**, 13.00 g, 13.72 mmoL) and $(Ph_3P)_2Cu(\mu\text{-}SEt)_2Ga(SEt)_2$ (SSP **2**, 6.67 g, 7.39 mmoL), dissolved in 100 mL of benzyl acetate in the presence of 1,2-ethanedithiol (2.4 mL, 28.50 mmoL) and 1-hexanethiol (20 mL, 142.1 mmoL). The reaction was heated at 195°C for 1 h. Upon completion, the reaction was cooled to room temperature, and $CuIn_{0.7}Ga_{0.3}S_2$ nanoparticles were recovered by serial precipitation, centrifugation, and washing in CH_3OH to provide red-black powder. This method has been successfully adapted to prepare up to 25 g of nanoparticles in a single vessel.

3. Results and Discussions

We recently reported the efficient microwave syntheses of highly cross-linked quaternary $CuIn_xGa_{1-x}S_2$ $(0 \leq x \leq 1)$ chalcopyrite nanoparticles in subgram scales. The method demonstrated high degrees of stoichiometric control by decomposing a mixture of two I–III bimetallic SSPs, $(Ph_3P)_2Cu(\mu\text{-}SEt)_2In(SEt)_2$ (**1**) and $(Ph_3P)_2Cu(\mu\text{-}SEt)_2Ga(SEt)_2$ (**2**), using 1,2-ethanedithiol as a cross-linker. The resulting nanoparticles could be engineered to exhibit bandgaps ranging from 1.59 to 2.30 eV by varying the amount of Ga in $CuIn_xGa_{1-x}S_2$ nanoparticles [11].

These highly cross-linked quaternary nanoparticles are insoluble in common organic solvents but retain individual nanoparticle characteristics such as phase, size, and bandgap. As expected, XRD peaks associated with chalcopyrite phase shift toward narrower lattice spacing, as a function of increasing amount of Ga [11].

In order to increase reproducibility of large-scale reactions, we chose $(Ph_3P)_2Cu(\mu\text{-}SPh)_2In(SPh)_2$ (SSP **3**) and $(Ph_3P)_2Cu(\mu\text{-}SPh)_2Ga(SPh)_2$ (SSP **4**) to be used in place of SSPs **1** and **2**. Due to their bulky and hydrophobic phenylthiolate ligands, SSPs **3** and **4** are more stable towards moisture and thermal decomposition compared to their ethylthiolate counterpart [33]. This allows for easier handling and greater reproducibility in larger reactions. The $CuIn_{0.7}Ga_{0.3}S_2$ nanoparticles have been synthesized (29 separate reactions resulting in about 150 g of nearly uniform nanoparticles under the same reaction conditions) from decomposition of SSPs **3** and **4** via microwave irradiation in the presence of 1,2-ethanedithiol at 200°C with high reproducibility.

The analysis of $CuIn_{0.7}Ga_{0.3}S_2$ nanoparticles by ICP-OES (Table 1) indicates that our method allows precise control of In/Ga ratio. The high level of control is likely due to the fact that 1,2-ethanedithiol acts as a bridging unit between two SSP units. This process produces cross-linked random polymers of SSPs, which undergo rapid decomposition to produce the resulting $CuIn_xGa_{1-x}S_2$ nanoparticles [14]. The ICP-OES data of $CuIn_{0.7}Ga_{0.3}S_2$ nanoparticles also show evidence of little or no change in the atomic percent of Cu, In, and Ga for all 29 reactions, Table 1. These results exhibit high reproducibility, improved product purities, and indicate that different forms of precursors can be used. The target formula of $CuIn_{0.7}Ga_{0.3}S_2$ was achieved by using 7 : 3 ratio of SSPs **3** and **4**.

FIGURE 2: Formation of soluble and insoluble CIGS nanoparticles from SSPs by controlling the ratio between 1,2-ethanedithiol and 1-hexanethiols.

TABLE 1: Representative sample compositions (from ICP-OES analysis) from 10 of 29 highly cross-linked $CuIn_{0.7}Ga_{0.3}S_2$ nanoparticle batches prepared at 200°C. *The standard deviation of all samples is 0.89 for Cu, 0.96 for In, and 0.35 for Ga.

Entry	Atomic percent (Raw)			In+Ga	In/In+Ga	Ga/In+Ga
	[Cu]*	[In]*	[Ga]*			
1	19.59	12.26	5.45	17.71	0.69	0.31
2	20.77	12.41	5.38	17.80	0.70	0.30
3	21.48	14.38	6.14	20.52	0.70	0.30
4	20.17	13.14	6.29	19.43	0.68	0.32
5	20.26	14.42	5.51	19.93	0.72	0.28
6	21.67	14.96	5.92	20.88	0.72	0.28
7	20.51	13.94	5.94	19.88	0.70	0.30
8	19.90	13.23	5.89	19.12	0.69	0.31
9	19.91	13.28	5.72	19.00	0.70	0.30
10	21.79	14.75	6.20	20.96	0.70	0.30

The estimated volume-weighted crystal diameters (employing Scherrer equation with a shape factor of 0.9) [34] of the $CuIn_{0.7}Ga_{0.3}S_2$ chalcopyrite nanoparticles samples are 4.4 ± 0.4 nm (Figure 3(a)). As shown in Figure 3(b), multiple batch samples exhibit almost identical absorption behavior with the average bandgap of 1.55 ± 0.05 eV.

Similar method can be used to prepare quaternary $CuIn_{0.7}Ga_{0.3}S_2$ chalcopyrite nanoparticles, which are soluble in common organic solvents such as hexanes, THF, and CH_2Cl_2. The increased solubility is attributed to the use of limited amount of 1,2-ethanedithiol in presence of excess 1-hexanethiol in the reaction mixture. Other monothiols with longer carbon chains and branched structures can also be used to modulate the resulting solubility.

From our previous experience, high-reaction temperature and/or the use of more than 2 equiv. of cross-linking agent is necessary to fully incorporate Ga to the crystalline structure. As shown in ICP-OES data (Table 2), Ga incorporation increases at higher reaction temperatures when 1:1 ratio of SSP **1** and **2** is used. However, the use of increasing amounts of 1,2-ethanedithiol leads to decreasing solubility, and the higher reaction temperatures result in larger particle sizes [11].

Thermogravimetric analyses (TGA/DSC-MS) of the soluble nanoparticles were performed at ambient pressure in alumina crucibles. The samples were heated at a rate of 10°C/min under an argon atmosphere. Weight loss was associated with decomposition of the passivation layers (Figure 4). Calculation of the derivative maximum rate of weight loss (MRW, %/°C) and step transition weight loss were used as a measure of relative stability. The TGA data show a smooth loss of mass over a temperature window of 250–400°C in two steps, accounting for a loss of 34.6%, 30.1%, and 28.4% for entries 11–13 (Table 2), respectively. The evolved gases were thermal decomposition products of 1,2-ethanedithiol and 1-hexanethiol as expected. These results are consistent with the ICP-OES analysis, a decrease in particle size results in a relative increase in the amount of organic material that makes up the passivation layer.

A bandgap range from 1.76 to 1.84 eV was obtained based on the absorption spectra. The estimated volume-weighted crystal diameters [34] of the $CuIn_xGa_{1-x}S_2$ chalcopyrite nanoparticles samples based on the XRD spectra are from 3.7 to 3.9 nm (Figure 5(a)). The photoluminescence emission (PLE) maxima increases can also be directly related to the increase in bandgap with increased Ga content (Figure 5(b)).

(a)

—— Entry 1	—— Entry 6
—— Entry 2	—— Entry 7
—— Entry 3	—— Entry 8
—— Entry 4	—— Entry 9
—— Entry 5	—— Entry 10

(b)
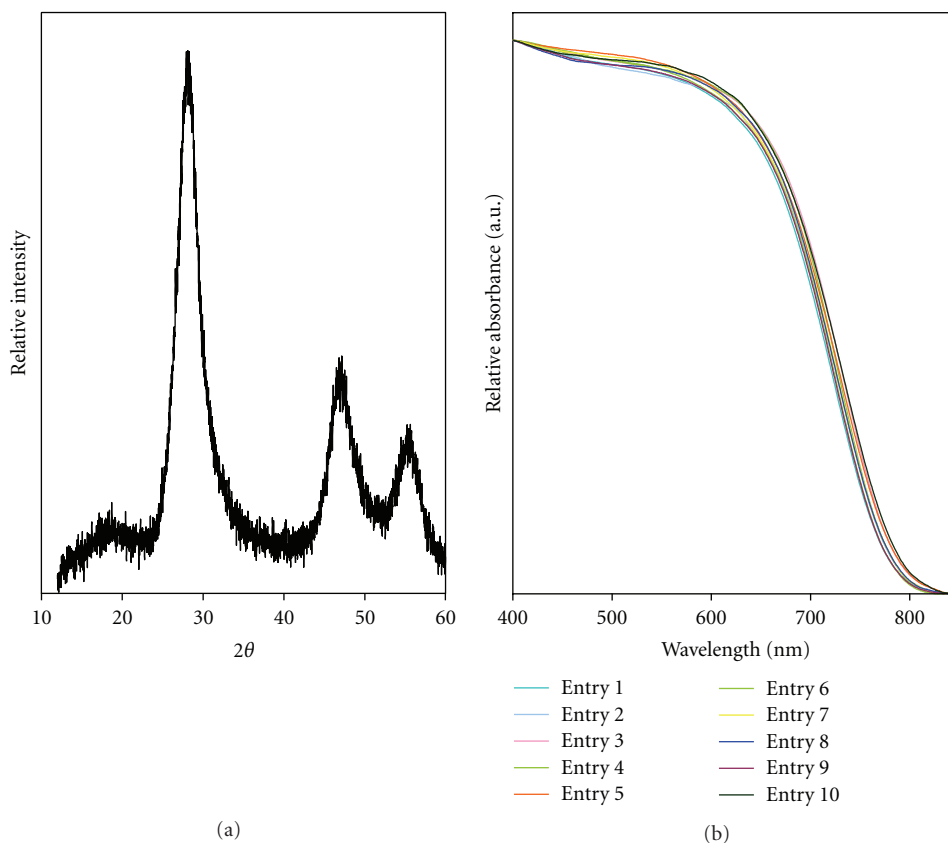
FIGURE 3: (a) Representative of normalized XRD data of $CuIn_{0.7}Ga_{0.3}S_2$ nanoparticles prepared at 200°C. (b) Normalized UV-Vis absorption spectra of typical $CuIn_{0.7}Ga_{0.3}S_2$ nanoparticles prepared at 200°C.

TABLE 2: Composition (from ICP-OES analysis) of soluble $CuIn_xGa_{1-x}S_2$ nanoparticles prepared at 160, 180, or 200°C.

Entry	Temp. (°C)	Cu%	In%	Ga%	In+Ga	In/In+Ga	Ga/In+Ga	MRW (%)
11	160	18.73	13.00	3.69	16.69	0.78	0.22	34.6
12	180	19.81	12.61	5.95	18.56	0.68	0.32	30.1
13	200	20.48	11.57	7.38	18.94	0.61	0.39	28.4
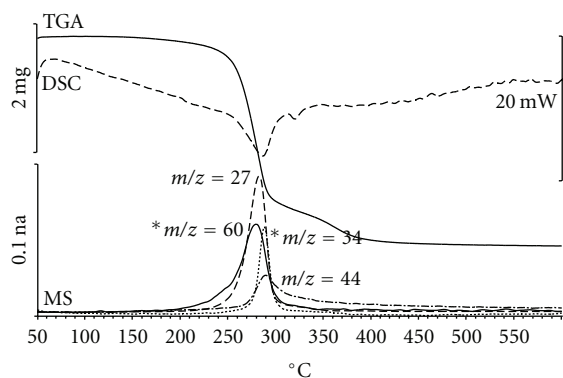
FIGURE 4: DSC/TGA-MS data for entry 11.

An HRTEM image of $CuIn_{0.61}Ga_{0.39}S_2$ nanoparticles (Table 2, entry 13) is shown in Figure 6. Observed sizes of $CuIn_{0.61}Ga_{0.39}S_2$ nanoparticles are 3.9 nm from HRTEM images which is consistent with the XRD-calculated size (Figure 5).

In order to demonstrate the reproducibility of the method, we also tried a scale-up version of the previous synthesis five times on a 5 g scale in 5 different reaction vessels to produce 25 g of soluble $CuIn_{0.72}Ga_{0.28}S_2$ nanoparticles at one time.

The analysis of $CuIn_xGa_{1-x}S_2$ nanoparticles by ICP-OES indicates that our method allows precise control of In and Ga ratio. The ICP-OES data of $CuIn_{0.72}Ga_{0.28}S_2$ nanoparticles also show evidence of little or no change in the atomic percent of Cu, In, and Ga for the reactions described in Table 3.

The average bandgap calculated from entries 14 through 18 is 1.78 ± 0.05 eV (Figure 7(b)). The estimated volume-weighted crystal diameters [29] of the $CuIn_{0.72}Ga_{0.28}S_2$ chalcopyrite nanoparticles samples are 4.1 ± 0.2 nm (Figure 7(a)).

(a)

(b)
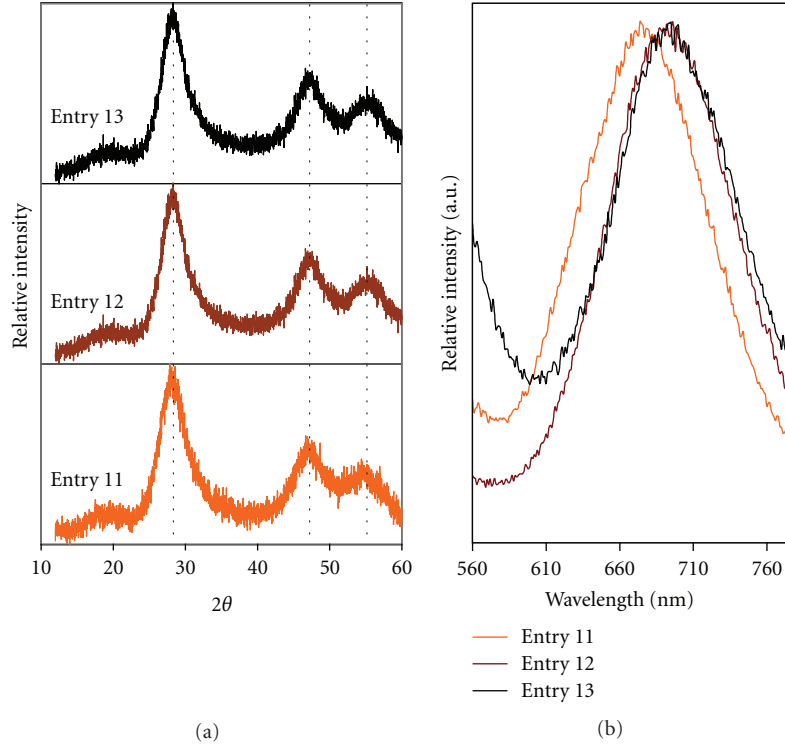
FIGURE 5: (a) Normalized XRD data of typical $CuIn_xGa_{1-x}S_2$ soluble nanoparticles prepared from 160 to 200°C. (b) Normalized photoluminescence spectra of typical $CuIn_xGa_{1-x}S_2$ soluble nanoparticles prepared from 160 to 200°C.

TABLE 3: Composition (from ICP-OES analysis), optical bandgaps (E_g) (from UV-Vis spectra), and sizes (from XRD) of soluble $CuIn_{0.72}Ga_{0.28}S_2$ nanoparticles prepared at 195°C.

Entry	Cu%	In%	Ga%	In+Ga	In/In+Ga	Ga/In+Ga	Eg (eV)	Size (nm)
14	21.77	14.85	5.59	20.44	0.73	0.27		
15	20.92	14.51	5.42	19.93	0.73	0.27		
16	21.47	14.23	5.28	19.50	0.73	0.27	1.78	4.1
17	20.99	13.53	5.76	19.29	0.70	0.30		
18	21.51	15.32	5.36	20.67	0.74	0.26		
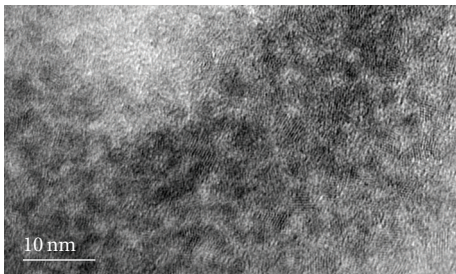
FIGURE 6: HRTEM image of $CuIn_{0.61}Ga_{0.39}S_2$ nanoparticles at 200°C.

4. Conclusion

The multigram scale synthesis of CIGS alloy nanoparticles is discussed. Potentially, these nanoparticles can be incorporated into next-generation quantum dot-based solar cells.

The ability to prepare quaternary $CuIn_xGa_{1-x}S_2$ ($0 \leq x \leq 1$) chalcopyrite nanoparticles with precise control of stoichiometry is important for controlling the bandgap and, therefore, the absorption behavior of the materials. The reaction temperatures are also critical for fine control of nanoparticle sizes and bandgaps. We have shown that by exploiting the microwave-assisted decomposition of two different SSPs in the presence of 1,2-ethanedithiol, we efficiently prepared $CuIn_xGa_{1-x}S_2$ ($0 \leq x \leq 1$) nanoparticles. Short reaction times of less than 1 hour have been achieved for the preparation of these nanoparticles. Two major advantages of this approach are precise stoichiometric control of In and Ga ratio and controlling the size of nanoparticles by reaction temperatures. A wide range of bandgaps can be engineered through a combination of precise control of elemental composition and particle sizes. We are currently exploring the use of various related SSPs to prepare multinary nanoparticles that exhibit an even wider range of bandgaps and other unique optoelectric behaviors.
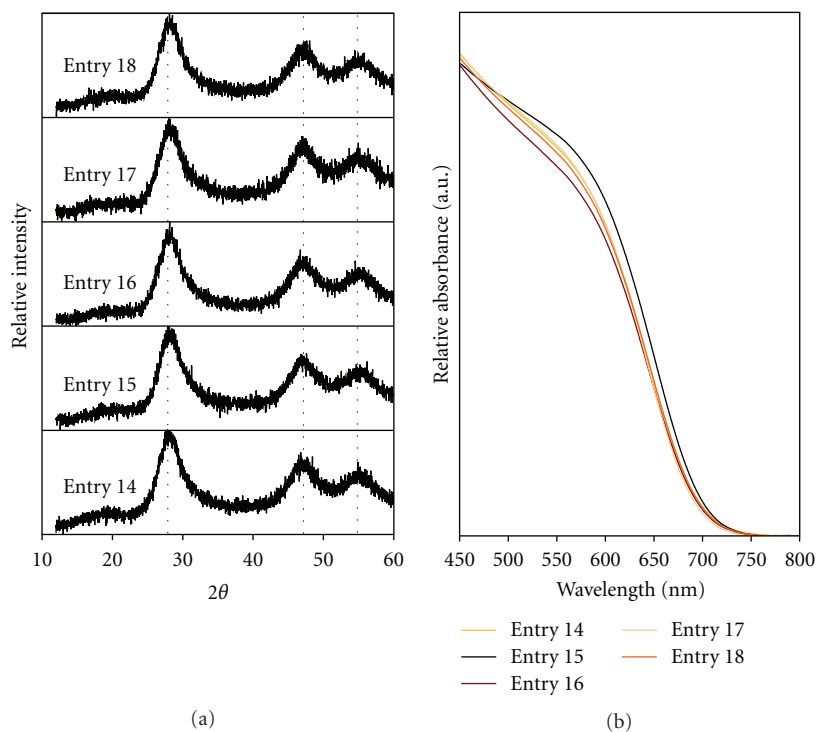
FIGURE 7: (a) Normalized XRD data of $CuIn_{0.72}Ga_{0.28}S_2$ soluble nanoparticles prepared 195°C. (b) Normalized UV-Vis absorption spectra of $CuIn_{0.72}Ga_{0.28}S_2$ soluble nanoparticles prepared 195°C.

Acknowledgments

References

[1] J. Tang, S. Hinds, S. O. Kelley, and E. H. Sargent, "Synthesis of colloidal $CuGaSe_2$, $CuInSe_2$, and $Cu(InGa)Se_2$ nanoparticles," *Chemistry of Materials*, vol. 20, no. 22, pp. 6906–6910, 2008.

[2] M. G. Panthani, V. Akhavan, B. Goodfellow et al., "Synthesis of $CuInS_2$, $CuInSe_2$, and $Cu(In_xGa_{1−x})Se_2$ (CIGS) nanocrystal "inks" for printable photovoltaics," *Journal of the American Chemical Society*, vol. 130, no. 49, pp. 16770–16777, 2008.

[3] S. Merdes, R. Sáez-Araoz, A. Ennaoui, J. Klaer, M. C. Lux-Steiner, and R. Klenk, "Recombination mechanisms in highly efficient thin film $Zn(S,O)/Cu(In,Ga)\,S_2$ based solar cells," *Applied Physics Letters*, vol. 95, no. 21, Article ID 213502, 2009.

[4] Q. Guo, G. M. Ford, H. W. Hillhouse, and R. Agrawal, "Sulfide nanocrystal inks for dense $Cu(In_{1−x}Ga_x)(S_{1−y}Se_y)_2$ absorber films and their photovoltaic performance," *Nano Letters*, vol. 9, no. 8, pp. 3060–3065, 2009.

[5] M. Yuan, D. B. Mitzi, W. Liu, A. J. Kellock, S. Jay Chey, and V. R. Deline, "Optimization of CIGS-based PV device through antimony doping," *Chemistry of Materials*, vol. 22, no. 2, pp. 285–287, 2010.

[6] I. Repins, M. A. Contreras, B. Egaas et al., "19.9%-efficient $ZnO/CdS/CuInGaSe_2$ solar cell with 81.2% fill factor," *Progress in Photovoltaics: Research and Applications*, vol. 16, no. 3, pp. 235–239, 2008.

[7] M. A. Green, K. Emery, Y. Hishikawa, and W. Warta, "Solar cell efficiency tables (version 36)," *Progress in Photovoltaics: Research and Applications*, vol. 18, no. 5, pp. 346–352, 2010.

[8] T. Todorov, E. Cordoncillo, J. F. Sánchez-Royo, J. Carda, and P. Escribano, "$CuInS_2$ films for photovoltaic applications deposited by a low-cost method," *Chemistry of Materials*, vol. 18, no. 13, pp. 3145–3150, 2006.

[9] S. Y. Lee and B. O. Park, "$CuInS_2$ thin films deposited by sol-gel spin-coating method," *Thin Solid Films*, vol. 516, no. 12, pp. 3862–3864, 2008.

[10] R. Motoyoshi, T. Oku, A. Suzuki, K. Kikuchi, and S. Kikuchi, "Fabrication and characterization of titanium dioxide/copper indium disulfide solar cells," *Journal of the Ceramic Society of Japan*, vol. 118, no. 1373, pp. 30–33, 2010.

[11] C. Sun, J. S. Gardner, G. Long et al., "Controlled stoichiometry for quaternary $CuIn_xGa_{1−x}\,S_2$ chalcopyrite nanoparticles from single-source precursors via microwave irradiation," *Chemistry of Materials*, vol. 22, no. 9, pp. 2699–2701, 2010.

[12] J. A. Gerbec, D. Magana, A. Washington, and G. F. Strouse, "Microwave-enhanced reaction rates for nanoparticle synthesis," *Journal of the American Chemical Society*, vol. 127, no. 45, pp. 15791–15800, 2005.

[13] J. Zhu, O. Palchik, S. Chen, and A. Gedanken, "Microwave assisted preparation of CdSe, PbSe, and $Cu_{2−x}Se$ nanoparticles," *Journal of Physical Chemistry B*, vol. 104, no. 31, pp. 7344–7347, 2000.

[14] C. Sun, J. S. Gardner, E. Shurdha et al., "A high yield synthesis of chalcopyrite $CuInS_2$ nanoparticles with exceptional size

control," *Journal of Nanomaterials*, vol. 2009, Article ID 748567, 7 pages, 2009.

[15] H. Grisaru, O. Palchik, A. Gedanken, V. Palchik, M. A. Slifkin, and A. M. Weiss, "Microwave-Assisted Polyol Synthesis of CuInTe$_2$ and CuInSe$_2$ Nanoparticles," *Inorganic Chemistry*, vol. 42, no. 22, pp. 7148–7155, 2003.

[16] T. Oku, A. Takeda, A. Nagata, T. Noma, A. Suzuki, and K. Kikuchi, "Fabrication and characterization of fullerene-based bulk heterojunction solar cells with porphyrin, CuInS$_2$, Diamond and exciton-diffusion blocking layer," *Energies*, vol. 3, no. 4, pp. 671–685, 2010.

[17] E. Arici, N. S. Sariciftci, and D. Meissner, "Hybrid solar cells based on nanoparticles of CuInS$_2$ in organic matrices," *Advanced Functional Materials*, vol. 13, no. 2, pp. 165–170, 2003.

[18] E. Arici, N. S. Sariciftci, and D. Meissner, "Photovoltaic properties of nanocrystalline CuInS$_2$/ methanofullerene solar cells," *Molecular Crystals and Liquid Crystals Science and Technology Section A*, vol. 385, pp. 129–136, 2002.

[19] E. Arici, H. Hoppe, F. Schäffler, D. Meissner, M. A. Malik, and N. S. Sariciftci, "Morphology effects in nanocrystalline CuInSe$_2$-conjugated polymer hybrid systems," *Applied Physics A*, vol. 79, no. 1, pp. 59–64, 2004.

[20] I. L. Medintz, H. T. Uyeda, E. R. Goldman, and H. Mattoussi, "Quantum dot bioconjugates for imaging, labelling and sensing," *Nature Materials*, vol. 4, no. 6, pp. 435–446, 2005.

[21] D. Shi, Y. Guo, Z. Dong et al., "Quantum-dot-activated luminescent carbon nanotubes via a nano scale surface functionalization for in vivo imaging," *Advanced Materials*, vol. 19, no. 22, pp. 4033–4037, 2007.

[22] S. Z. Kang, Y. K. Yang, W. Bu, and J. Mu, "TiO$_2$ nanoparticles incorporated with CuInS$_2$ clusters: preparation and photocatalytic activity for degradation of 4-nitrophenol," *Journal of Solid State Chemistry*, vol. 182, no. 11, pp. 2972–2976, 2009.

[23] S. L. Castro, S. G. Bailey, R. P. Raffaelle, K. K. Banger, and A. F. Hepp, "Synthesis and characterization of colloidal CuInS$_2$ nanoparticles from a molecular single-source precursor," *Journal of Physical Chemistry B*, vol. 108, no. 33, pp. 12429–12435, 2004.

[24] S. L. Castro, S. G. Bailey, R. P. Raffaelle, K. K. Banger, and A. F. Hepp, "Nanocrystalline chalcopyrite materials (CuInS$_2$ and CuInSe 2) via low-temperature pyrolysis of molecular single-source precursors," *Chemistry of Materials*, vol. 15, no. 16, pp. 3142–3147, 2003.

[25] T. C. Deivaraj, J. H. Park, M. Afzaal, P. O'Brien, and J. J. Vittal, "Novel bimetallic thiocarboxylate compounds as single-source precursors to binary and ternary metal sulfide materials," *Chemistry of Materials*, vol. 15, no. 12, pp. 2383–2391, 2003.

[26] J. J. Nairn, P. J. Shapiro, B. Twamley et al., "Preparation of ultrafine chalcopyrite nanoparticles via the photochemical decomposition of molecular single-source precursors," *Nano Letters*, vol. 6, no. 6, pp. 1218–1223, 2006.

[27] H. Zhong, Y. Zhou, M. Ye et al., "Controlled synthesis and optical properties of colloidal ternary chalcogenide CuInS$_2$ nanocrystals," *Chemistry of Materials*, vol. 20, no. 20, pp. 6434–6443, 2008.

[28] M.-Y. Chiang, S.-H. Chang, C.-Y. Chen, F.-W. Yuan, and H.-Y. Tuan, "Quaternary CuIn(S$_{1-x}$Se$_x$)$_2$ nanocrystals: facile heating-up synthesis, band gap tuning, and gram-scale production," *The Journal of Physical Chemistry C*, vol. 115, no. 5, pp. 1592–1599, 2011.

[29] H. Zhong, S. S. Lo, T. Mirkovic et al., "Noninjection gram-scale synthesis of monodisperse pyramidal CuInS$_2$ nanocrystals and their size-dependent properties," *ACS Nano*, vol. 4, no. 9, pp. 5253–5262, 2010.

[30] K. K. Banger, M. H. C. Jin, J. D. Harris, P. E. Fanwick, and A. F. Hepp, "A new facile route for the preparation of single-source precursors for bulk, thin-film, and nanocrystallite I-III-VI semiconductors," *Inorganic Chemistry*, vol. 42, no. 24, pp. 7713–7715, 2003.

[31] W. Hirpo, S. Dhingra, A. C. Sutorik, and M. G. Kanatzidis, "Synthesis of mixed copper-indium chalcogenolates. single-source precursors for the photovoltaic materials CuInQ$_2$ (Q = S, Se)," *Journal of the American Chemical Society*, vol. 115, no. 4, pp. 1597–1599, 1993.

[32] K. R. Margulieux, C. Sun, L. N. Zakharov, A. W. Holland, and J. J. Pak, "Stepwise introduction of thiolates in copper-indium binuclear complexes," *Inorganic Chemistry*, vol. 49, no. 9, pp. 3959–3961, 2010.

[33] C. Sun, R. D. Westover, K. R. Margulieux, L. N. Zakharov, A. W. Holland, and J. J. Pak, "Divergent syntheses of copper-indium bimetallic single-source precursors via thiolate ligand exchange," *Inorganic Chemistry*, vol. 49, no. 11, pp. 4756–4758, 2010.

[34] H. Natter, M. Schmelzer, M. S. Löffler, C. E. Krill, A. Fitch, and R. Hempelmann, "Grain-growth kinetics of nanocrystalline iron studied in situ by synchrotron real-time X-ray diffraction," *Journal of Physical Chemistry B*, vol. 104, no. 11, pp. 2467–2476, 2000.